Probabilistic Engineering Mechanics 44 (2016) 28–34

Contents lists available at ScienceDirect

Probabilistic Engineering Mechanics

journal homepage: www.elsevier.com/locate/probengmech

Variability response functions for apparent material properties

Sanjay R. Arwade [a,*], George Deodatis [b], Kirubel Teferra [c]

[a] Department of Civil & Environmental Engineering, University of Massachusetts, 130 Natural Resources Road, Amherst, MA 01003, USA
[b] Department of Civil Engineering & Engineering Mechanics, Columbia University, USA
[c] Multifunctional Materials Branch, US Naval Research Laboratory, USA

ARTICLE INFO

Article history:
Received 14 August 2015
Accepted 19 October 2015
Available online 24 October 2015

Keywords:
Homogenization
Effective properties
Apparent properties
Finite element analysis
Random heterogeneous materials
Variability response function
Probabilistic mechanics

ABSTRACT

The computation of apparent material properties for a random heterogeneous material requires the assumption of a solution field on a finite domain over which the apparent properties are to be computed. In this paper the assumed solution field is taken to be that defined by the shape functions that underpin the finite element method and it is shown that the variance of the apparent properties calculated using the shape functions to define the solution field can be expressed in terms of a variability response function (VRF) that is independent of the marginal distribution and spectral density function of the underlying random heterogeneous material property field. The variance of apparent material properties can be an important consideration in problems where the domain over which the apparent properties are computed is smaller than the representative volume element and the approach introduced here provides an efficient means of calculating that variance and performing sensitivity studies with respect to the characteristics of the material property field. The approach is illustrated using examples involving heat transfer problems and finite elements with linear and nonlinear shape functions and in one and two dimensions. Features of the VRF are described, including dependency on shape and scale of the finite element and the order of the shape functions.

1. Introduction

In the practical analysis of engineering problems using continuum approaches, apparent, effective, or homogenized material properties must be computed to apply the governing equations of continuum mechanics. When an apparent material property is computed in a given domain from an underlying random field model for a spatially varying material property the result is a random quantity that is no longer spatially variable. For example, apparent elastic modulus or thermal conductivity are random variables that are spatially constant over the problem domain as opposed to the underlying spatially varying random fields. As the volume of the domain increases, the variance of the apparent properties decreases until it becomes negligible, at which point one is said to have reached the representative volume element (RVE). For many structural and mechanical systems, assumption of an RVE is appropriate, but for many others residual uncertainty in the apparent properties should be considered. This situation has, to some extent, been characterized as involving the statistical volume element (SVE) [1–3] and addressed using Monte Carlo based finite element approaches [4–6]. This paper describes a method for computing the variability of apparent material properties—specifically the thermal conductivity—using variability response functions (VRFs) that have the advantage of being analytically rather than numerically derived and provide a method for computing the variance of the apparent property that is independent of the distribution and spectrum of the underlying material property field. In the context of this paper, the VRF formulation is developed by imposing the shape functions of the finite element formulation on the problem domain and computing apparent properties based on equivalence of the finite element characteristic matrices for the heterogeneous and homogeneous versions of the problem.

One of the challenges present in any approach to computing apparent properties is that the apparent property obtained depends on the boundary conditions applied to the heterogeneous version of the problem in obtaining the apparent property [7,8]. Using the shape functions of a finite element formulation does not remove this boundary condition dependence, but does allow the obtained apparent properties to be, in a sense, consistent with the formulation used in further finite element analysis of the problem. Other approaches commonly used include the imposition of periodic boundary conditions [9].

The VRF approach to uncertainty quantification was developed in the context of computing the variance of the displacement response of structural systems with spatially varying, random material properties [10–12]. It has since been extended to the problem

* Corresponding author.
E-mail address: arwade@umass.edu (S.R. Arwade).

http://dx.doi.org/10.1016/j.probengmech.2015.10.010
0266-8920/

of computing the variance of apparent elastic material properties for statically determinate, indeterminate, and continuum systems [8,13,14]. Here, those approaches are combined with the seminal approach to the stochastic finite element method that computes the variability of the nodal displacements in a finite element model based on an underlying stochastic field of material properties [12].

The remainder of the paper is organized as follows: First a problem statement is given that defines more precisely the notion of the apparent material property and the residual uncertainty associated with the apparent property. Next the general approach to computing VRFs for the apparent material properties in a finite element context is introduced for the heat conduction problem. Examples are then given for the linear and quadratic one dimensional elements and the linear triangular element. Finally, comments are provided on how this version of assessing the uncertainty of apparent properties may find a place in a multi-scale analysis context.

2. Problem statement

Let $\Omega \subset \mathbb{R}^n$ define a solid body occupied by a material with properties defined by the spatially varying and random (heterogeneous) matrix $\mathbf{c}(\mathbf{x})$, $\mathbf{x} \in \mathbb{R}^n$ and subject to Neumann and Dirichlet boundary conditions on the boundary segments $\partial\Omega_{neumann}$ and $\partial\Omega_{dirichlet}$ respectively. Consider now the case in which this body, subject to the same boundary conditions, is occupied by a material with properties defined by the spatially invariant (homogeneous) matrix $\bar{\mathbf{c}}$. The definition of an apparent property depends on choosing $\bar{\mathbf{c}}$ such that

$$g(\phi_{het}(\mathbf{x})) = g(\phi_{hom}(\mathbf{x})) \tag{1}$$

where $\phi_{het}(\mathbf{x})$ and $\phi_{hom}(\mathbf{x})$ are solution fields in the heterogeneous and homogeneous bodies respectively and $g(\cdot)$ represents a function of those solution fields that is usually chosen to have some physical meaning. In elasticity problems the strain energy is often chosen to act as $g(\cdot)$ so that the energetics of the heterogeneous and homogeneous versions of the problem are equivalent. Other rational choices, however, can be made. For example, in a heat transfer problem $g(\cdot)$ could be chosen to be the temperature at a particular point of importance in the problem, and similarly in an elasticity problem a key displacement could be selected. The matrix $\bar{\mathbf{c}}$ of apparent material properties is itself stochastic, unless Ω is a representative volume element (RVE) but not spatially varying. The primary interest in this paper is computation of the uncertainty associated with $\bar{\mathbf{c}}$, when the problem domain is a finite volume smaller than the RVE. Beyond the fact that the solution $\bar{\mathbf{c}}$ to Eq. (1) is itself stochastic, that solution depends on the specific boundary conditions applied in computing $\phi_{het}(\mathbf{x})$ and $\phi_{hom}(\mathbf{x})$. This dependence of apparent material properties on boundary conditions represents a significant challenge to developing consistent and widely applicable definitions of apparent properties. Most currently available approaches involve assumption of periodic boundary conditions or the assumption of a form for the solution field. In this paper, the second approach is taken, but in a novel way involving the use of the shape functions associated with finite elements used to solve practical problems numerically.

In this paper, a stochastic scheme for computing apparent properties is proposed for the scalar field problem of heat conduction in one, two, or three spatial dimensions with a single material property defining a constitutive matrix that is physically isotropic and is also statistically homogeneous and isotropic. That is, the solution field is the temperature $\phi(\mathbf{x}) = t(\mathbf{x})$ and the material property is the thermal conductivity $\mathbf{c}(\mathbf{x}) = \lambda(\mathbf{x})$. The randomness in the problem can be modeled as $\lambda(\mathbf{x}) = \lambda(\mathbf{x})\lambda^*$ in which $\lambda(\mathbf{x}) = \lambda_0(1 + f(\mathbf{x}))$ is a random field composed of a mean value λ_0 and a random part $f(\mathbf{x})$, a mean zero, statistically homogeneous and isotropic random field characterized by its spectral density $S_{ff}(\boldsymbol{\kappa})$, $\boldsymbol{\kappa} \in \mathbb{R}^n$ where $\boldsymbol{\kappa}$ is a vector of wave numbers. For the case of heat conduction, the constitutive matrix of the homogeneous problem is $\bar{\lambda} = \bar{\lambda}\lambda^*$ and the goal of this paper is to evaluate the uncertainty in $\bar{\lambda}$ by developing efficient means of computing $\mathrm{var}[\bar{\lambda}]$. Specifically, the goal is to develop a variability response function for $\mathrm{var}[\bar{\lambda}]$ such that

$$\mathrm{var}[\bar{\lambda}] = \int_{[-\infty,\infty]^n} \mathrm{VRF}_{\bar{\lambda}}(\boldsymbol{\kappa}) S_{ff}(\boldsymbol{\kappa})\, d\boldsymbol{\kappa} \tag{2}$$

where $\mathrm{VRF}_{\bar{\lambda}}(\boldsymbol{\kappa})$ is a VRF for the apparent conductivity that is independent of the distribution and spectrum of $f(\mathbf{x})$.

3. Finite element based VRFs for apparent conductivity

A finite element is defined by its geometry and the shape functions used to interpolate the solution field within the element domain. In this paper the element domain is $\Omega \subset \mathbb{R}^n$ and the shape functions are denoted by $\mathbf{N} = [N_1(\mathbf{x}), \ldots, N_m(\mathbf{x})]$ where m is the number of nodes the element possesses. In the case of the scalar field heat transfer problem, m is also the total number of degrees of freedom in the element. The gradients of the shape functions are denoted by $\mathbf{B}$, an $n \times m$ matrix with components $B_{ij} = \partial N_j(\mathbf{x})/\partial x_i$ for the heat transfer problem. The conductivity matrix for the heterogeneous version of the problem is $\lambda(\mathbf{x}) = \lambda_0(1 + f(\mathbf{x}))\mathbf{I}$ where I is the $n \times n$ identity matrix, and the conductivity matrix of the homogeneous version of the problem is $\lambda = \bar{\lambda}\mathbf{I}$.

Given these definitions, and further defining $\mathbf{B}^* = \mathbf{B}^T\mathbf{B}$ for compactness of notation, the characteristic matrices of the homogeneous and heterogeneous versions of the problem can be defined as

$$\mathbf{k}_{hom} = \bar{\lambda} \int_\Omega \mathbf{B}^*(\mathbf{u})\, d\mathbf{u} \tag{3}$$

$$\mathbf{k}_{het} = \lambda_0 \int_\Omega \mathbf{B}^*(\mathbf{u})(1 + f(\mathbf{u}))\, d\mathbf{u}. \tag{4}$$

Except in the case where $\mathbf{B}^*$ is a constant matrix—corresponding to linear shape functions—it is not possible to define a single value of $\bar{\lambda}$ using $\mathbf{k}_{het} = \mathbf{k}_{hom}$. Therefore a matrix of apparent conductivities $\bar{\lambda}$ such that

$$\bar{\lambda}_{ij} = \frac{\lambda_0}{\int_\Omega B^*_{ij}(\mathbf{u})\, d\mathbf{u}} \times \int_\Omega B^*_{ij}(\mathbf{u})(1 + f(\mathbf{u}))\, d\mathbf{u} \tag{5}$$

defines the components of a matrix that contains a set of apparent material properties.

The mean of $\bar{\lambda}_{ij}$ is obtained by

$$E[\bar{\lambda}_{ij}] = \frac{\lambda_0}{\int_\Omega B^*_{ij}(\mathbf{u})\, d\mathbf{u}} \times E\left[\int_\Omega B^*_{ij}(\mathbf{u})(1 + f(\mathbf{u}))\, d\mathbf{u}\right] \tag{6}$$

$$E[\bar{\lambda}_{ij}] = \frac{\lambda_0}{\int_\Omega B^*_{ij}(\mathbf{u})\, d\mathbf{u}} \times \int_\Omega B^*_{ij}(\mathbf{u}) E[(1 + f(\mathbf{u}))]\, d\mathbf{u} \tag{7}$$

$$E[\bar{\lambda}_{ij}] = \lambda_0 \tag{8}$$

since $E[f(\mathbf{u})] = 0$ and $B^*_{ij}(\mathbf{u})$ is deterministic. The variance is $\mathrm{var}[\bar{\lambda}_{ij}] = E[\bar{\lambda}^2_{ij}] - E[\bar{\lambda}_{ij}]^2$. Calculation of the second moment $E[\bar{\lambda}^2_{ij}]$, the remaining quantity needed to calculate the variance, begins with

$$\bar{\lambda}_{ij}^2 = \frac{\lambda_0^2}{\iint_\Omega B_{ij}^*(\mathbf{u})B_{ij}^*(\mathbf{v})\,d\mathbf{u}\,d\mathbf{v}} \times \iint_\Omega B_{ij}^*(\mathbf{u})B_{ij}^*(\mathbf{v}) \times (1+f(\mathbf{u}))(1+f(\mathbf{v}))\,d\mathbf{u}\,d\mathbf{v} \tag{9}$$

$$\bar{\lambda}_{ij}^2 = \frac{\lambda_0^2}{\iint_\Omega B_{ij}^*(\mathbf{u})B_{ij}^*(\mathbf{v})\,d\mathbf{u}\,d\mathbf{v}} \times \iint_\Omega B_{ij}^*(\mathbf{u})B_{ij}^*(\mathbf{v}) \times (1+f(\mathbf{u})+f(\mathbf{v})+f(\mathbf{u})f(\mathbf{v}))\,d\mathbf{u}\,d\mathbf{v}. \tag{10}$$

Applying the expectation operator gives

$$E[\bar{\lambda}_{ij}^2] = \frac{\lambda_0^2}{\iint_\Omega B_{ij}^*(\mathbf{u})B_{ij}^*(\mathbf{v})\,d\mathbf{u}\,d\mathbf{v}} \times \iint_\Omega B_{ij}^*(\mathbf{u})B_{ij}^*(\mathbf{v})(1+R_{ff}(\boldsymbol{\xi}))\,d\mathbf{u}\,d\mathbf{v} \tag{11}$$

where $R_{ff}(\boldsymbol{\xi})$ is the spatial correlation function of $f(\mathbf{x})$ and $\boldsymbol{\xi} \in \mathbb{R}^n$ is a vector of separation distances with $\xi_i = u_i - v_i$. The variance can therefore be expressed in terms of the shape function gradients contained in $\mathbf{B}^*$, the mean conductivity λ_0, and the correlation function $R_{ff}(\boldsymbol{\xi})$ as

$$\mathrm{var}[\bar{\lambda}_{ij}] = \frac{\lambda_0^2}{\iint_\Omega B_{ij}^*(\mathbf{u})B_{ij}^*(\mathbf{v})\,d\mathbf{u}\,d\mathbf{v}} \times \iint_\Omega B_{ij}^*(\mathbf{u})B_{ij}^*(\mathbf{v})R_{ff}(\boldsymbol{\xi})\,d\mathbf{u}\,d\mathbf{v}. \tag{12}$$

The Wiener–Khintchine relations allow substitution of the spectral density for the correlation function so that the variance can be expressed as

$$\mathrm{var}[\bar{\lambda}_{ij}] = \frac{\lambda_0^2}{\iint_\Omega B_{ij}^*(\mathbf{u})B_{ij}^*(\mathbf{v})\,d\mathbf{u}\,d\mathbf{v}} \times \iint_\Omega B_{ij}^*(\mathbf{u})B_{ij}^*(\mathbf{v}) \times \int_{[-\infty,\infty]^n} e^{-i\boldsymbol{\xi}\cdot\boldsymbol{\kappa}} S_{ff}(\boldsymbol{\kappa})\,d\boldsymbol{\kappa}\,d\mathbf{u}\,d\mathbf{v} \tag{13}$$

in which it is important to note that $\boldsymbol{\xi}$ is a function of $\mathbf{u}$ and $\mathbf{v}$ for the purposes of integration in the space domain. By changing the order of integration and grouping terms, the variance can be expressed in the form of a VRF as

$$\mathrm{var}[\bar{\lambda}_{ij}] = \int_{[-\infty,\infty]^n} \mathrm{VRF}_{\bar{\lambda}_{ij}}(\boldsymbol{\kappa}) S_{ff}(\boldsymbol{\kappa})\,d\boldsymbol{\kappa} \tag{14}$$

with

$$\mathrm{VRF}_{\bar{\lambda}_{ij}} = \frac{\lambda_0^2}{\iint_\Omega B_{ij}^*(\mathbf{u})B_{ij}^*(\mathbf{v})\,d\mathbf{u}\,d\mathbf{v}} \times \iint_\Omega B_{ij}^*(\mathbf{u})B_{ij}^*(\mathbf{v})e^{-i\boldsymbol{\xi}\cdot\boldsymbol{\kappa}}\,d\mathbf{u}\,d\mathbf{v}. \tag{15}$$

This key expression allows the variance of the apparent conductivity within the finite element to be calculated exactly without Monte Carlo simulation or the application of any approximations, many of which limited to situations in which the magnitude of the uncertainty is relatively small. Furthermore, the VRF is independent of the spectrum and marginal distribution of $f(\mathbf{x})$ and therefore the VRF need only be calculated once and can then be used to compute the variance of the apparent conductivity for any underlying stochastic field with minimal computational effort provided the spectral properties are available.

A significant issue with the results of Eqs. (14) and (15) is that, in general, $\bar{\lambda}_{ij} \neq \bar{\lambda}_{kl}$ and therefore the approach of equating components of $\mathbf{k}_{het}$ and $\mathbf{k}_{hom}$ does not provide a unique definition of the apparent conductivity. One approach to establishing a single value for the apparent conductivity is to define a linear combination of the components of $\bar{\lambda}$ such that

$$\bar{\bar{\lambda}} = \sum_{i=1,j=i}^{m} W_{ij}\bar{\lambda}_{ij}, \qquad \sum_{i=1,j=i}^{m} W_{ij} = 1 \tag{16}$$

where W_{ij} are weights that could be computed, for example, to minimize the error in the apparent conductivity across a range of applied boundary conditions. As before, the primary interest of this paper is in the variance of $\bar{\bar{\lambda}}$ which, since it is a linear combination of the components of $\bar{\lambda}$, is

$$\mathrm{var}[\bar{\bar{\lambda}}] = \sum_{i=1,j=i} W_{ij}^2\,\mathrm{var}[\bar{\lambda}_{ij}] \tag{17}$$

implying that a VRF exists for the variance of $\bar{\bar{\lambda}}$ such that

$$\mathrm{var}[\bar{\bar{\lambda}}] = \int_{[-\infty,\infty]^n} \mathrm{VRF}_{\bar{\lambda}}(\boldsymbol{\kappa}) S_{ff}(\boldsymbol{\kappa})\,d\boldsymbol{\kappa} \tag{18}$$

and

$$\mathrm{VRF}_{\bar{\lambda}}(\boldsymbol{\kappa}) = \sum_{i=1,j=i}^{m} W_{ij}^2 \mathrm{VRF}_{\bar{\lambda}_{ij}\bar{\lambda}_{kl}}(\boldsymbol{\kappa}) \tag{19}$$

with

$$\mathrm{VRF}_{\bar{\lambda}_{ij}\bar{\lambda}_{kl}}(\boldsymbol{\kappa}) = \frac{\lambda_0^2}{\iint_\Omega B_{ij}^*(\mathbf{u})B_{kl}^*(\mathbf{v})\,d\mathbf{u}\,d\mathbf{v}} \times \iint_\Omega B_{ij}^*(\mathbf{u})B_{kl}^*(\mathbf{v})e^{-i\boldsymbol{\xi}\cdot\boldsymbol{\kappa}}\,d\mathbf{u}\,d\mathbf{v} \tag{20}$$

and $\mathrm{VRF}_{\bar{\lambda}_{ij}\bar{\lambda}_{kl}} = \mathrm{VRF}_{\bar{\lambda}_{ij}}$ when $(k,l) = (i,j)$. Thus, the VRF for the combined apparent conductivity is simply the weighted sum of the VRFs for the individual components of $\bar{\lambda}$.

4. Examples

4.1. One dimensional linear element

For a one-dimensional element ($n=1$) with two linear shape functions ($m=2$), the terms B_{ij}^* become constants and can be taken outside the integrals in Eqs. (5) and (15), meaning that $\bar{\lambda}_{ij} = \bar{\lambda}_{kl}$ and

$$\mathrm{VRF}_{\bar{\lambda}}(\kappa) = \mathrm{VRF}_{\bar{\lambda}_{ij}}(\kappa) = \frac{\lambda_0^2}{L^2}\int_0^L \int_0^L e^{-i\kappa(u-v)}\,du\,dv = \left(\frac{2\lambda_0}{\kappa L}\right)^2 \sin^2\left(\frac{\kappa L}{2}\right) \tag{21}$$

where L is the length of the element. This VRF is shown in Fig. 1. Note that for the linear one dimensional element, the VRF is a function of κL, the number of waves of property variation

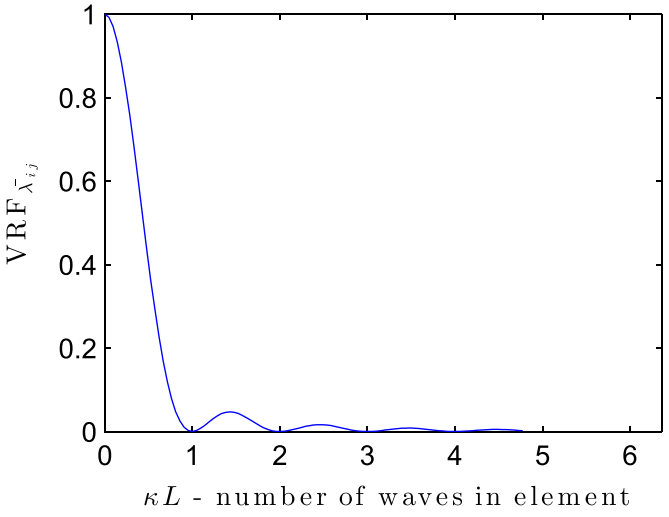

Fig. 1. VRF for the one dimensional linear heat element.

contained in the element. As is typical of VRFs, the spectral contribution to variance peaks at $\kappa=0$ and exhibits a decaying sequence of peaks with increasing wave number.

4.2. One dimensional quadratic element

Consider now a one dimensional ($n=1$) element with 3 nodes and quadratic shape functions ($m=3$). In this case, since the components of $\mathbf{B}^*$ are not constants, the term $\mathbf{B}^*_{ij}(\mathbf{u})\mathbf{B}^*_{kl}(\mathbf{v})$ cannot be brought outside the integral in Eq. (15) and $\bar{\lambda}_{ij} \neq \bar{\lambda}_{kl}$. Let the coordinates of the three nodes of the element be $x^{(1)}=0$, $0 < x^{(2)} < x^{(3)}$, and $x^{(3)}=L$. This section describes the form of the VRFs for $\bar{\lambda}_{11}$, $\bar{\lambda}_{22}$, and $\bar{\lambda}_{33}$ and the dependence of those VRFs on the location of $x^{(2)}$, the interior node of the element. It is also shown how a linear combination of those three apparent conductivities also has a VRF for its variance. The diagonal terms of $\bar{\bar{\lambda}}$ are chosen for examination because they are the terms corresponding to the characteristic matrix coefficients that capture the work done in applying the canonical boundary conditions for computation of the component of the characteristics matrix. That is, k_{11} is derived by setting $T_1=1$, $T_2=T_3=0$ and computing the heat flux needed at node 1 to maintain that temperature distribution. Similar calculations are performed for k_{22} and k_{33}. Fig. 2(a) shows the VRFs for the diagonal entries of $\bar{\bar{\lambda}}$ for the case when $x^{(2)}=L/2$. It can be seen that due to symmetry in the problem $\mathrm{VRF}_{\bar{\lambda}_{11}}(\kappa)=\mathrm{VRF}_{\bar{\lambda}_{33}}(\kappa)$. Fig. 2 (b) shows the same VRFs computed for an element with the interior node located at $x^{(2)}=L/3$. Note that when $x^{(2)}=L/3$, the symmetry of the element is broken and $\mathrm{VRF}_{\bar{\lambda}_{11}}(\kappa) \neq \mathrm{VRF}_{\bar{\lambda}_{33}}(\kappa)$.

Finally, since for the quadratic one dimensional element, $\bar{\lambda}_{ij} \neq \bar{\lambda}_{kl}$, it is instructive to see the form of a VRF for the apparent conductivity $\bar{\bar{\lambda}}$ as defined in Eq. (16) with $W_{11}=W_{22}=W_{33}=1/3$, $W_{12}=W_{13}=W_{23}=0$ so that the apparent property is the arithmetic average of the diagonal entries of $\bar{\bar{\lambda}}$. Fig. 3 shows $\mathrm{VRF}_{\bar{\bar{\lambda}}}(\kappa)$ both for the case when $x^{(2)}=L/2$ and when $x^{(2)}=L/3$. The averaging procedure renders the VRFs very similar in this case.

4.3. Two dimensional linear element: Linear triangle

The simplest two dimensional ($n=2$) finite element is the linear triangle (also known as the T3 element) which has three nodes, (m=3), located at $\{\mathbf{x}^{(1)}, \mathbf{x}^{(2)}, \mathbf{x}^{(3)}\}$ and three associated shape functions

$$N_1(\mathbf{x}) = \frac{1}{2A}((x_1^{(2)}x_2^{(3)} - x_1^{(3)}x_2^{(2)}) + (x_{2,2}^{(2)} - x_2^{(3)})x_1 + (x_1^{(3)} - x_1^{(2)})x_2)$$
$$N_2(\mathbf{x}) = \frac{1}{2A}((x_1^{(3)}x_2^{(1)} - x_1^{(1)}x_2^{(3)}) + (x_2^{(3)} - x_2^{(1)})x_1 + (x_1^{(1)} - x_1^{(3)})x_2)$$
$$N_3(\mathbf{x}) = \frac{1}{2A}((x_1^{(1)}x_2^{(2)} - x_1^{(2)}x_2^{(1)}) + (x_2^{(1)} - x_2^{(2)})x_1 + (x_1^{(2)} - x_1^{(1)})x_2). \quad (22)$$

For this element, as for the one dimensional linear element, the shape functions are linear in $\mathbf{x}$ and therefore $\mathbf{B}$ is a constant matrix and B^*_{ij} can be taken outside the integrals in Eqs. (5) and (15). This results in direct calculation of the VRF for the linear triangle as

$$\mathrm{VRF}_{\bar{\bar{\lambda}}}(\boldsymbol{\kappa}) = \frac{\lambda_0^2}{A^2}\iint_\Omega e^{-i(\kappa_1(u_1-u_2)+\kappa_2(v_1-v_2))}\,du_1\,du_2\,dv_1\,dv_2 \quad (23)$$

where $A=\iint_\Omega d\mathbf{x}$ is the area of the element. For a two dimensional element, the VRF is a function of two wave numbers κ_1 and κ_2 and may in general depend on the shape and size of the element. In the following, therefore, VRFs for a series of example triangular elements are presented to illustrate these dependencies. An obvious and potentially useful extension to the current work would be to develop the apparent property VRF in the natural coordinate system of the family of isoparametric elements. Developing such an isoparametric formulation is planned by the

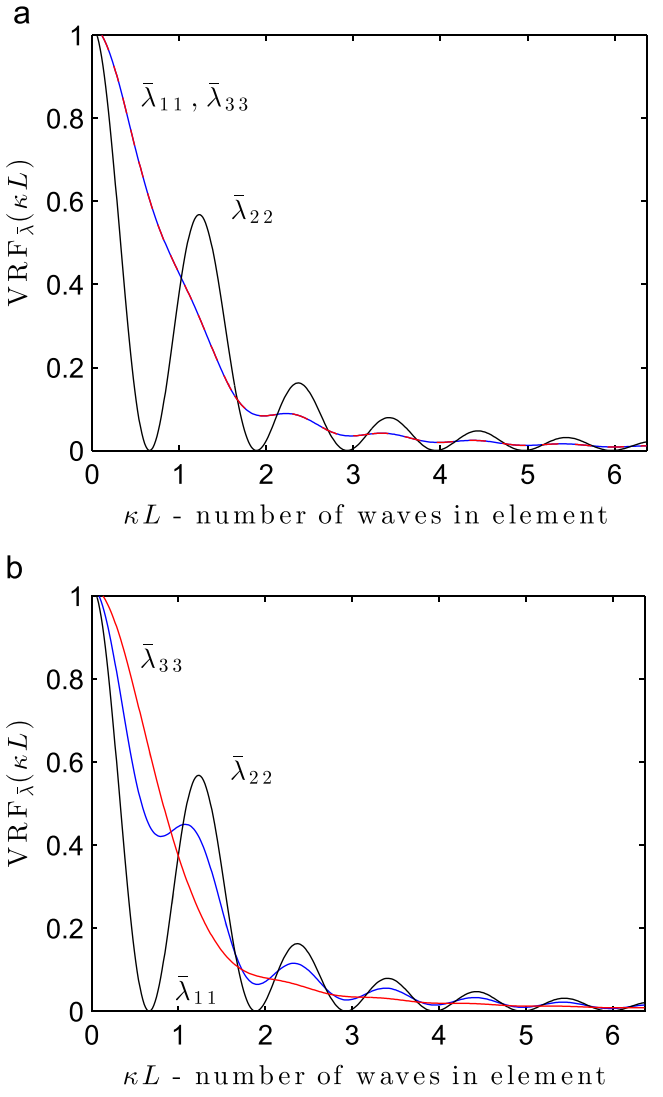

Fig. 2. VRFs of diagonal components of $\bar{\lambda}$ for the one dimensional quadratic element. (a) VRFs for diagonal components of $\bar{\lambda}$ for $x^{(2)}=L/2$. (b) VRFs for diagonal components of $\bar{\lambda}$ for $x^{(2)}=L/3$.

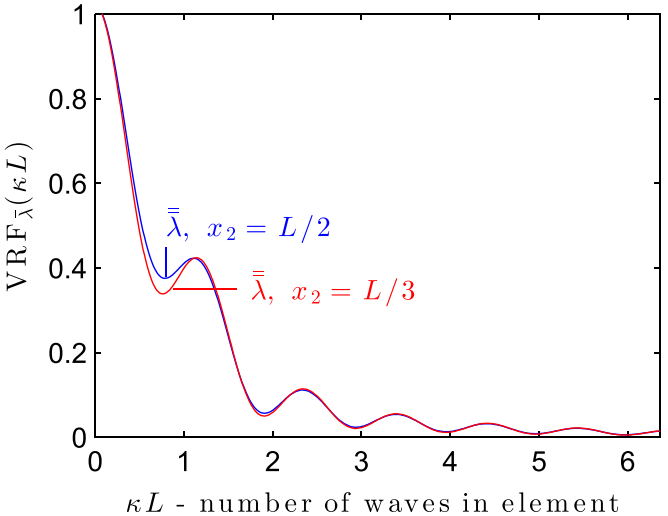

Fig. 3. VRFs for $\bar{\bar{\lambda}}$ for $x^{(2)}=L/2$ and $x^{(2)}=L/3$ for the one-dimensional quadratic element.

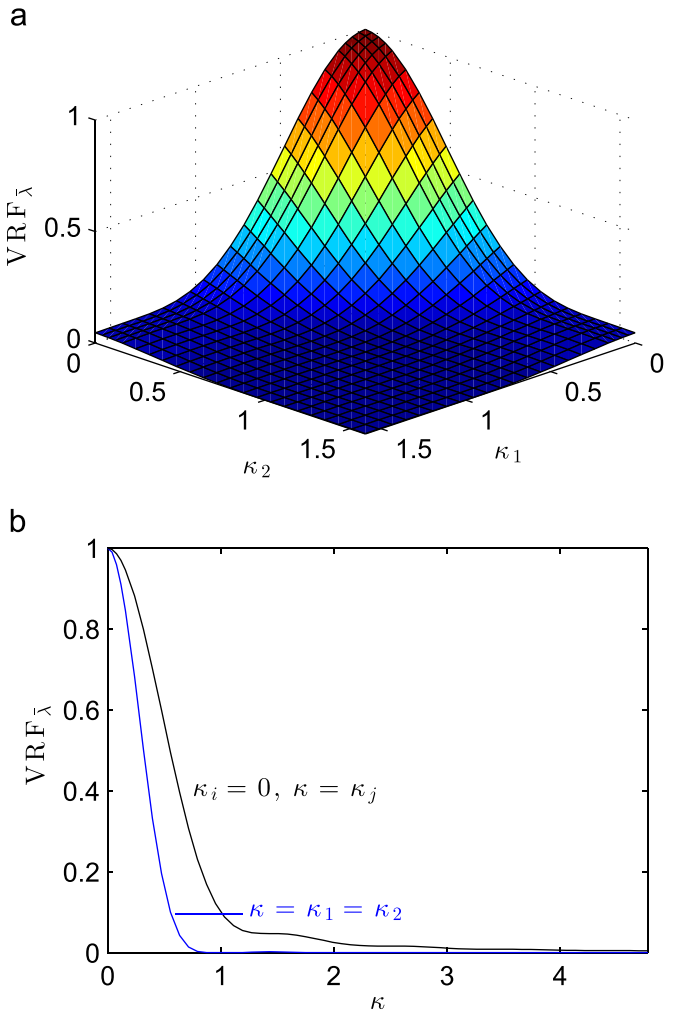

Fig. 4. VRF for linear triangular element with $\mathbf{x}^{(1)} = (0, 0)$, $\mathbf{x}^{(2)} = (1, 0)$, and $\mathbf{x}^{(3)} = (1, 1)$. (a) Overall VRF surface. (b) Sections through VRF surface. Diagonal section $\kappa_1 = \kappa_2$ and edge section $\kappa_i = 0$, $\kappa = \kappa_j$.

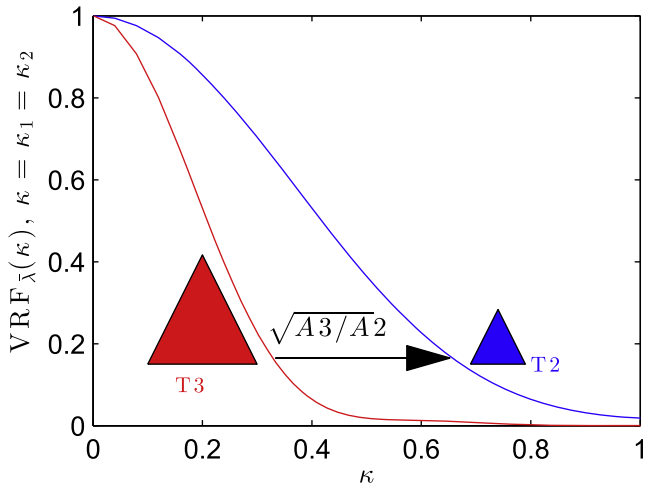

Fig. 5. VRFs for similar isosceles triangles T2 and T3 showing that VRFs for similar triangles coincide with proper scaling of the wavenumber.

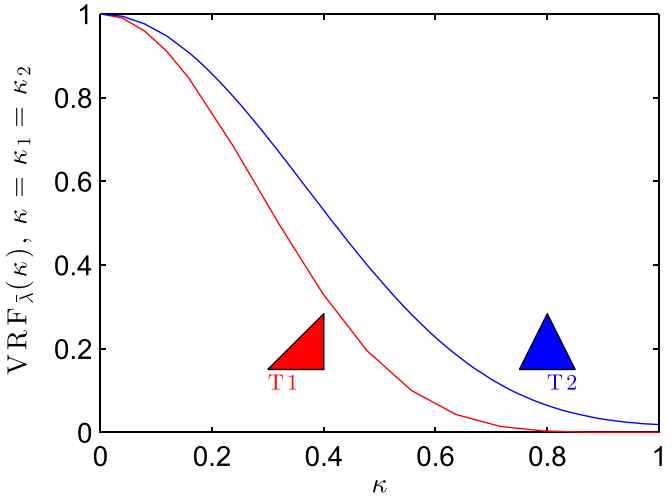

Fig. 6. VRFs for equal area triangles T1 and T2 showing that VRFs for equal area triangles depend on the maximum side length.

authors.

Consider first the right triangular element T1 with vertices at $\mathbf{x}^{(1)} = (0, 0)$, $\mathbf{x}^{(2)} = (1, 0)$, and $\mathbf{x}^{(3)} = (1, 1)$. The apparent property VRF, $\mathrm{VRF}_{\bar{\lambda}}(\boldsymbol{\kappa})$, is shown in Fig. 4(a) with sections through the surface obtained by setting $\kappa = \kappa_1 = \kappa_2$ and $\kappa_i = 0$, $\kappa = \kappa_j$ shown separately in Fig. 4(b). Results show most of the usual characteristics of VRFs with a peak at κ=0 and asymptotic values of $\lim_{|\boldsymbol{\kappa}|\to\infty} \mathrm{VRF}_{\bar{\lambda}}(\boldsymbol{\kappa}) = 0$. A significant contrast with the VRFs developed for one dimensional elements is that for the linear triangle, the decay of the VRF towards its asymptotic value is essentially monotonic whereas for the one dimensional elements there are oscillations about the general asymptotic trend of decay (see Figs. 1 and 2). The lack of oscillations in the linear triangle is caused by averaging of the fluctuating material properties over a two dimensional domain with non-rectilinear shape that therefore does not contain integer numbers of waves in the fluctuating random property field. As shown by the two section curves (Fig. 4 (b)) the VRF is not isotropic in the $\boldsymbol{\kappa}$ space. Specifically, the decay rate of the VRF is faster along the $\kappa_1 = \kappa_2$ diagonal than along the κ_i axes. When $\kappa_i = 0$, $\kappa = \kappa_j$, there are material property fluctuations in only one of the coordinate directions and therefore the apparent property has a greater variance associated with it than when $\kappa_1 = \kappa_2$ and there are equal wave number fluctuations in both coordinate directions.

Although the VRF is defined analytically and uniquely for the linear triangular element, there remain factors of shape and scale that may influence the form of the VRF. The following discussion addresses those issues. For clarity and simplicity of the figures that follow, the VRFs for a series of linear triangular element shapes are presented in the form of the diagonal sections with $\kappa = \kappa_1 = \kappa_2$.

First, to address the question of scale, the VRF is computed for two similar isosceles triangles with vertices at $\mathbf{x}^{(1)} = (0, 0)$, $\mathbf{x}^{(2)} = (1, 0)$, and $\mathbf{x}^{(3)} = (1/2, 1)$ (T2) and $\mathbf{x}^{(1)} = (0, 0)$, $\mathbf{x}^{(2)} = (2, 0)$, and $\mathbf{x}^{(3)} = (1, 2)$ (T3). The diagonal sections of these VRFs shown in Fig. 5 demonstrate, as expected, that the VRFs for similar triangular elements can be made to coincide by scaling the wave number by

$$\mathrm{VRF}_{\bar{\lambda}}^{(T2)}(\boldsymbol{\kappa}) = \mathrm{VRF}_{\bar{\lambda}}^{(T3)}(\boldsymbol{\kappa}^*)$$
$$\boldsymbol{\kappa}^* = \boldsymbol{\kappa}\sqrt{\frac{A_2}{A_3}} \tag{24}$$

where A_2 is the area of T2 and A_3 is the area of T3.

Next, to address the question of shape, consider two triangles with equal area, one the isosceles triangle T2 and one the right triangle T1. Fig. 6 shows the VRFs for these two elements and demonstrates a sensitivity of the VRF not only to area of the element but also to shape. The VRF of the right triangle decays faster

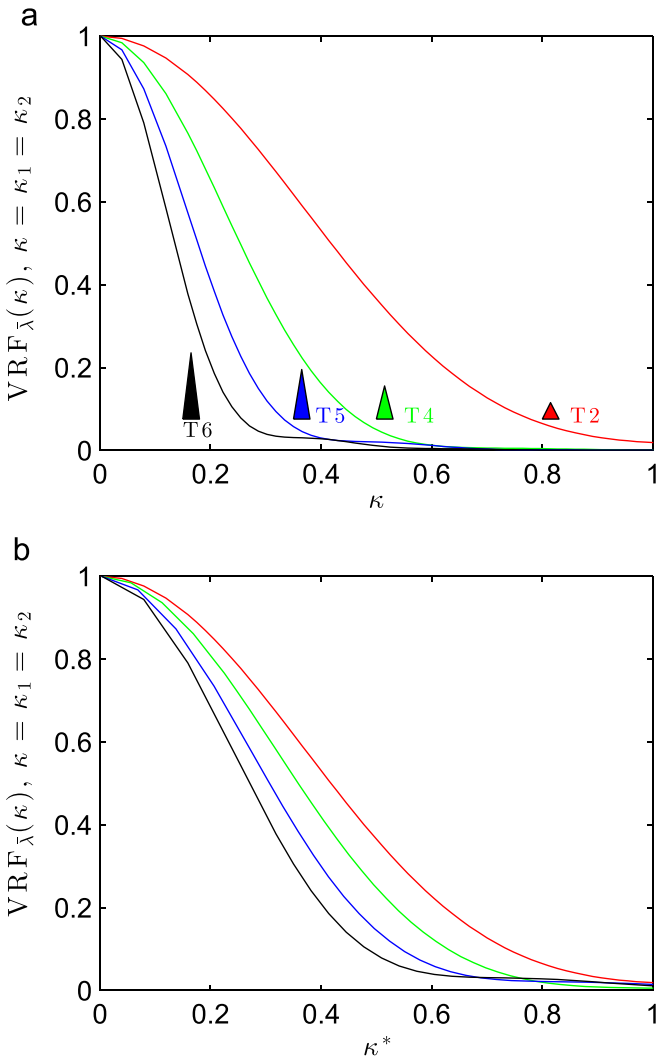

Fig. 7. Effect of aspect ratio on VRFs. (a) VRFs for varying aspect ratio triangles. Note that triangles are shown to a different scale than in previous figures so as not to interfere with plot lines. (b) VRFs for varying aspect ratio triangles plotted against scaled wavenumber. Order of curves is the same as in part (a) of the figure.

than that for the isosceles triangle. This appears to be a result of the longer maximum side length in T1 as opposed to T2. In T1, the hypotenuse has length of 1.41, whereas in T2 the maximum side length is 1.12. Although the element areas are identical, the presence of a longer side length enhances the stability of the apparent material property and thereby reduces the variance.

A final consideration is that of the aspect ratio of the triangular element, illustrated by Fig. 7, in which the VRFs for elements T2 and T4 ($\mathbf{x}^{(1)} = (0, 0)$, $\mathbf{x}^{(2)} = (1, 0)$, $\mathbf{x}^{(3)} = (1/2, 2)$), T5 ($\mathbf{x}^{(1)} = (0, 0)$, $\mathbf{x}^{(2)} = (1, 0)$, $\mathbf{x}^{(3)} = (1/2, 3)$) and T6 ($\mathbf{x}^{(1)} = (0, 0)$, $\mathbf{x}^{(2)} = (1, 0)$, $\mathbf{x}^{(3)} = (1/2, 4)$) are provided. Part (a) of the figure shows that as the height of the element increases, the VRF decays more rapidly with wave number. This is largely a function of the increasing area of the triangle. Close examination of the lower part of the VRF curves reveals that the curves are not simply shifted and self-similar (as in Fig. 5), but rather the large aspect ratio elements begin to exhibit small oscillations in the decay as present for the one-dimensional elements (Figs. 1 and 2). This phenomenon arises because as the element aspect ratio increases, the element begins to approach a one-dimensional domain and the VRF begins to resemble that for a one-dimensional element. The role of aspect ratio is highlighted by part (b) of the figure, in which the VRFs are plotted against κ^*, the scaled wavenumber as defined in Eq. (24). After scaling of the wavenumber, the VRFs do not coincide either in location (due to side length) or shape (due to aspect ratio).

The illustrations presented above demonstrate that although the VRF is defined uniquely and analytically for a linear triangle with general geometry, the form and scale of the VRF depends significantly on the geometry of the element. Even when scaling is applied to the wavenumber based on element area, there remain differences between the VRFs for different elements. This poses a potential challenge for implementation of VRF estimation of material property variability in a finite element context in that a different VRF must be computed for each element. There are, however, several approaches that could render the use of the VRF in a two dimensional finite element context tractable. Among these are:

1. Simply compute the VRF for each element in a mesh. Because the VRF is defined analytically, this should not be overly taxing in a computational sense, and it may in fact prove most efficient to compute the integral definition of the VRF using a Gauss quadrature procedure run in parallel to computation of the element characteristic matrices.
2. Compute a single VRF for all elements in a mesh based on some definition of the average element shape and size. This corresponds roughly and conceptually to using an average of the scaled VRFs in Fig. 7(b). This approach would introduce error in the variance estimates, but for well constructed meshes this error should be relatively small.

Finally, it should be noted that the dependence of the VRF on element shape represents a further motivation for constructing meshes with well formed elements of consistent size, shape, and aspect ratio since doing so not only yields better conditioning of the characteristic matrices but also smaller element-to-element variation in the VRFs.

5. Discussion

5.1. Application to assessing deterministic property assumption

It is a common practice in FEA to assume that it is sufficient to derive the element characteristic matrix from the mean constitutive relation (i.e. the finite element is larger than the RVE). The analytical VRF enables a very practical approach to assessing the validity of this assumption by computing the variance of the apparent properties for a given SDF. For one dimension, an element length of L_x corresponds to a minimum wave number of $\kappa_{min} = 2\pi/L_x$ and thus

$$\mathrm{var}[\bar{\lambda}_{ij}] = \int_{2\pi/L_x}^{\infty} \mathrm{VRF}_{\bar{\lambda}_{ij}}(\kappa) S_{ff}(\kappa)\, d\kappa < \epsilon_{thresh} \tag{25}$$

provides a criterion to assess the RVE assumption for a given SDF. It should be noted that this is not sufficient to determine the size of the RVE because the element shape functions impose a solution field that may not be resolved enough to accurately account for the fluctuations of the material properties. Rather, satisfaction of Eq. (25) for small ϵ_{thresh} is a necessary criterion in order to solely utilize mean apparent properties when conducting FEA.

5.2. Towards a multi-scale framework

Computation of apparent properties over a finite element rather than over an entire body also provides a direct approach to stochastic upscaling of material properties for multiscale analysis. Consider a body discretized into finite elements Ω_i with a random,

spatially varying, material property field $\lambda(\mathbf{x})$. Using the approaches described in the previous sections, it is possible to model the material property field within each element as a random variable $\bar{\bar{\lambda}}_i$ with mean value λ_0 and variance calculated according to Eq. (18). At the crudest level, one could treat the random variables $\bar{\bar{\lambda}}_i$ as independent. However, this is not likely to be a useful approach since if the elements are large enough that independence between $\bar{\bar{\lambda}}_i$ and $\bar{\bar{\lambda}}_j$ can be assumed, the elements will be approaching the RVE in size and the variance of $\bar{\bar{\lambda}}_i$ will be very small. Instead, one must incorporate medium to long range correlations into the upscaled model. One approach involves the centroids of the finite elements, denoted as $\mathbf{c}_i$. Since the material property within each element is being treated as a random variable, a covariance matrix can be computed with components

$$R_{ij} = \lambda_0^2 R_{ff}(\mathbf{c}_i - \mathbf{c}_j). \tag{26}$$

If the distribution of $\bar{\bar{\lambda}}_i$ can be computed or approximated—perhaps as Gaussian since $\bar{\bar{\lambda}}_i$ is the result of integration of a random field—samples of the set of random variables $\{\bar{\bar{\lambda}}_i\}$ can be generated having the appropriate medium and long range correlation structure.

5.3. Definition of a single apparent property

Recall that for an element with nonlinear shape functions the apparent property, and therefore its associated VRF is not uniquely defined. In order to allow treatment of the homogeneous version of the problem with a single apparent property Eq. (16) introduced a weighted sum of the components of the apparent property matrix and in the example that followed a simple version of this unified apparent property, in which the diagonal components of $\bar{\lambda}$ were combined with equal weights. Consider the series of cases $W_{ij} = 1,\ W_{kl} = 0, (k, l) \neq (i, j)$, in which $\bar{\bar{\lambda}}$ is set equal to one of the components of $\bar{\lambda}$. Using this approximation would result in error between the heterogeneous and homogeneous versions of the problem for all but the set of boundary conditions corresponding to $\bar{\lambda}_{ij}$. In further work on this topic, then, it is anticipated that the weights W_{ij} of Eq. (16) could be chosen through an optimization procedure that minimizes error (perhaps in terms of energy) between the heterogeneous and homogeneous versions of the problem across the suite of all possible boundary conditions that may be imposed on the element. The simple example presented here is meant primarily to illustrate that an apparent property VRF can be defined analytically for $\bar{\bar{\lambda}}$ and that the resulting VRF is less dependent on element characteristics than are the components of $\bar{\lambda}$.

6. Conclusion

By imposing prescribed temperature fields defined by element shape functions on a finite element domain, it has been shown that apparent conductivities can be obtained by equating components of the characteristic matrix derived for an element with random, spatially varying material properties and an equivalent element with spatially constant material properties. Except in the case of linear shape functions, however, it is not possible to define a single, unique value for the apparent conductivity since it depends on the applied boundary conditions or temperature field. In such cases, a number of apparent conductivities can be defined equal to the number of distinct entries of the characteristic matrix. The expected values of these apparent conductivities are identical, but the variances differ and can be calculated using a VRF approach. A linear combination of the distinct apparent conductivities can be defined that also has a variance expressed through a VRF. Three sets of examples have been presented: linear one-dimensional, quadratic one-dimensional, and linear two-dimensional. The linear one-dimensional example illustrated the basic method of computation of the VRF and some features of its form; the quadratic one-dimensional element illustrates the non-uniqueness of the VRF for higher order elements and; the linear two-dimensional element illustrated the shape and scale dependence of the VRF.

References

[1] M. Ostoja-Starzewski, Microstructural randomness versus representative volume element in thermomechanics, J. Appl. Mech.—Trans. ASME 69 (1) (2002) 25–35 , UT: WOS:000175343900004.
[2] M. Ostoja-Starzewski, Material spatial randomness: from statistical to representative volume element, Probab. Eng. Mech. 21 (2) (2006) 112–132 , International Conference on Heterogeneous Material Mechanics (ICHMM), June 21–26, 2004, Chongqing, PR China; UT: WOS:000237863200002.
[3] T. Kanit, S. Forest, I. Galliet, V. Mounoury, D. Jeulin, Determination of the size of the representative volume element for random composites: statistical and numerical approach, Int. J. Solids Struct. 40 (1314) (2003) 3647–3679 , UT: WOS:000183361300025.
[4] P.D. Spanos, A. Kontsos, A multiscale Monte Carlo finite element method for determining mechanical properties of polymer nanocomposites, Probab. Eng. Mech. 23 (2008) 456–470.
[5] P.D. Spanos, P. Elsbernd, B. Ward, et al., Estimation of the physical properties of nanocomposites by finite-element discretization and Monte Carlo simulation, Philos. Trans. R. Soc. A 371.
[6] P.D. Spanos, S.K. Georgantzinos, N.K. Anifantis, Mechanical properties of graphene nanocomposites: a multiscale finite element prediction, Compos. Struct. 132 (2015) 536–544.
[7] D.H. Pahr, P.K. Zysset, Influence of boundary conditions on computed apparent elastic properties of cancellous bone, Biomech. Model. Mechanobiol. 7 (6) (2008) 463–476 , UT: WOS:000259670700003.
[8] S.R. Arwade, G. Deodatis, Variability response functions for effective material properties, Probab. Eng. Mech. 26 (2) (2011) 174–181 , UT: WOS:000289825700007.
[9] L. Graham, S. Baxter, Simulation of local material properties based on moving-window gmc, Probab. Eng. Mech. 16 (4) (2001) 295–305 , Conference on Monte Carlo Simulation, June 18–21, 2000; Monte Carlo, Monaco; UT: WOS:000172053600005.
[10] F. Wall, G. Deodatis, Variability response functions of stochastic plane-stress strain problems, J. Eng. Mech.—ASCE 120 (9) (1994) 1963–1982 , UT: WOS: A1994PC79400009.
[11] L. Graham, G. Deodatis, Variability response functions for stochastic plate bending problems, Struct. Saf. 20 (2) (1998) 167–188 , UT: WOS:000074679100004.
[12] G. Deodatis, Weighted integral method. 1. Stochastic stiffness matrix, J. Eng. Mech.—ASCE 117 (8) (1991) 1851–1864 , UT: WOS:A1991FY42600011.
[13] K. Teferra, S.R. Arwade, G. Deodatis, Stochastic variability of effective properties via the generalized variability response function, Comput. Struct. 110 (2012) 107–115 , UT: WOS:000310114500008.
[14] K. Teferra, S.R. Arwade, G. Deodatis, Generalized variability response functions for two-dimensional elasticity problems, Comput. Methods Appl. Mech. Eng. 272 (2014) 121–137 , UT: WOS:000334481100007.